Simulation of the January 2014 flood on the Secchia River using a fast and high-resolution 2D parallel shallow-water numerical scheme

Simulation of the January 2014 flood on the Secchia River using a fast and high-resolution 2D parallel shallow-water numerical scheme

RENATO VACONDIO, PhD, Research Fellow *Department of Civil and Environmental Engineering and Architecture, University of Parma, Parco Area delle Scienze 181/A, 43124 Parma, Italy*

Email: renato.vacondio@unipr.it

FRANCESCA AURELI, PhD, Research Assistant, *Department of Civil and Environmental Engineering and Architecture, University of Parma, Parco Area delle Scienze 181/A, 43124 Parma, Italy*

Email: francesca.aureli@unipr.it

ALESSIA FERRARI, PhD Student, *Department of Civil and Environmental Engineering and Architecture, University of Parma, Parco Area delle Scienze 181/A, 43124 Parma, Italy*

Email: alessia.ferrari3@studenti.unipr.it

PAOLO MIGNOSA, PhD, Full Professor, *Department of Civil and Environmental Engineering and Architecture, University of Parma, Parco Area delle Scienze 181/A, 43124 Parma, Italy*

Email: paolo.mignosa@unipr.it

ALESSANDRO DAL PALÙ, PhD, Professor, *Department of Mathematics and Computer Science, University of Parma, Parco Area delle Scienze 53/A, 43124 Parma, Italy*

Email: alessandro.dalpalu@unipr.it

Abstract

The capability of a GPU-parallelized numerical scheme to produce accurate and fast simulations of floodings induced by levee-breach in large domains, adopting high resolution Digital Terrain Maps (DTMs), is investigated. The good predictive skills of the presented 2D shallow water model were proven with regard to the inundation caused by a levee breach occurred on the Secchia River, Italy in January 2014. The numerical computations were carried out on a domain of about 180 square kilometers adopting a Cartesian grid of approximately 7.2 Mcells with size 5 m. The results of the simulation were validated against several field data and observations, including a high resolution Synthetic Aperture Radar image. A ratio between simulation and physical times of about 1/15 was achieved; this kind of simulation tools opens up new perspectives in the devising and implementing of flood event management strategies for civil protection purposes and with the aim of minimizing the economic loss.

Introduction

In the recent years trends in flood frequencies and flooding damage appear to be increasing with a consequent worsening of the social and economic repercussions. According to Jongman et al. (2014), from 2000 to 2012 flooding events in Europe caused losses for about 4.9 billion euros every year, and the latest inundations of 2013 (central Europe and UK) brought damages of 12 billion euros. Moreover, owing to climate change, flooding events are expected to double by 2050 and global losses to increase till more than 500%. Similarly Hallegatte et al. (2013) underline how global flood losses will achieve in 2050 the value of 52 billion dollars per year and considering the climate change they estimate annual losses to reach 1 trillion dollars per year. Hence, the development and application of tools capable to provide accurate and fast predictions for flood management is crucial to obtain a reduction of the damages caused by floods. Several analyses have been carried out to demonstrate that 2D shallow water numerical models can be proficiently applied to the simulation of flood events also with the aim of designing measures to prevent flood damage. After having involved specialists and decision-makers, Leskens et al. (2014) concluded that flood simulation models are not yet used by decision makers as widely as it could be expected. This is mainly ascribed to the fact that the computational time of traditional 2D shallow-water numerical models is still excessive and also to the fact that the numerical models are not yet flexible enough to adapt to real situations. This well-known problem has led the researchers to investigate different modelling approaches in the attempt to speed up their computations without loss of accuracy. For example Horritt and Bates (2002) investigated different predictive performances of 1D and 2D models in estimating the inundation extents by studying a 60 km reach of Severn River (UK). Focusing the attention to flooding events due to levee breaches, Masoero et al. (2013) and Di Baldassarre et al. (2009) studied respectively the 1951 and 1879 historical inundations on the Po River in Northern Italy. Mazzoleni et al. (2014) analyzed synthetic scenarios to define the flood hazard due to levee breaches. Domeneghetti et al. (2013) analyzed the effect of several unavoidable sources of uncertainty that characterize the models of inundations triggered by levee breaches. In all these analyses the river is described by means of a 1D model, used also to compute the discharge hydrograph flowing through the levee breach, this hydrograph is then adopted as inflow boundary condition for the 2D numerical scheme of the flood-prone area. This means that 2D simulations are then performed only in the plains outside the river region. The main motivation for the adoption of this approach lies in the necessity to reduce the computational time: creating a fully 2D models of both the river region and the flood–prone area entails in fact a high computational effort. However, often the flow in the river region cannot be accurately described through 1D numerical schematization due to the presence of a main channel which meanders within the valley limits and since close to the breach the velocity in the direction normal to the thalweg is not negligible. Moreover the adoption of two different non-linked numerical schemes for the river and the flood-prone area does not allow to model properly backwater effects which can have a significant influence on the discharge flowing through the breach.

Some authors have proposed to develop 1D-2D coupled numerical schemes (Gejadze & Monnier 2007, Bladé et al. 2012, Morales-Hernández et al. 2013, Morales-Hernández et al. 2014) to overcome the limitation described before. In those models the river region is discretized by means of cross-sections whereas the 2D model is used to describe the large areas outside the river region, where the 1D assumptions does not hold. When coupled models are adopted special care has to be made to define the boundary conditions for the 1D and the 2D models in such a way that both global mass and momentum are conserved at the coupling zones (Morales-Hernández et al. 2013). Moreover in such models the region where the 1D approximation holds has to be defined a priori.

As pointed out by Leskens et al. (2014), the adoption of two different numerical schematizations makes the use of numerical models much more complex and less flexible for flood disaster management. To overcome these limitations, already manifest in the recent past, Aureli and Mignosa (2004) and Aureli et al. (2006) developed fully 2D numerical models of both the river region and the flood prone areas for the modelling of flooding scenarios due to levee breaches in the Po River, although with low spatial resolution.

Until recently the traditional surveying techniques allowed the description of river reaches mainly through series of cross sections and terrain data outside the river banks were usually provided at a low resolution, adequate to that exploitable at the time by the modelling tools. An accurate high resolution modelling of flows was, as consequence, barely achievable. More recently Light Detection and Ranging (LiDAR) and Digital Terrain Models (DTM) with spatial resolution of 1–3 m and elevation accuracy of 10 cm have become more and more widespread and are now available for many flood prone areas. As an example more than 62% of England and Wales (81% of urban areas) is covered by LiDAR surveys (Di Baldassarre and Uhlenbrook 2012). This represents a revolution for flood risk modeling.

Schumann et al. (2014) pointed out how the availability of high resolution DTMs can dramatically enhance the capability of flood modeling at local scale, offering the chance of obtaining accurate maps of the risk related to flood disasters. Marks and Bates (2000), Gallegos et al. (2009) and Dottori et al. (2013) analyzed the effect of spatial resolution on 1D and 2D flood modeling, highlighting the capability of shallow–water models to simulate inundations in urban and sub-urban areas when high resolution is used. However high resolution simulations entail considerable computational costs.

Sanders et al. (2010) presented a parallel shallow-water numerical model based on Message Passing Interface (MPI) technique which allows remarkable speedups (ratios between the sequential computational time over the GPU parallel time for the same code). Alternative to this approach is the adoption of GPU-parallelized codes using CUDA programming language. The advantages of the GPU parallelization, with respect to a traditional MPI framework, are the significantly decreased cost per processor and the efficient on-card communication. Whereas MPI communication requires large supercomputers, which are very expensive to buy and to maintain, GPU cards can be installed on standard desktop computers. The parallelization of 2D Shallow Water Equations models has been presented in the past by different authors (Crossley et al 2010, Brodtkorb et al. 2012, De la Asunción et al. 2013, Lacasta et al. 2014, Vacondio et al. 2014 and Lacasta et al. 2015) for structured and non-structured grids.

High resolution modelling of floods induced by levee breach is here analyzed adopting an original GPU-parallelized model implemented by Vacondio et al. 2014 and based on an explicit Shock–Capturing Finite Volume method for the solution of the 2D Shallow Water equations. Speedups of two orders of magnitude are thus achieved. Thanks to this efficient parallelization the issues related to long computational times are addressed; moreover the river and the flood prone areas are integrated in a single computational domain and the flow phenomenon is modelled as a whole avoiding the special treatments proper of linked 1D and 2D numerical schemes. To illustrate the capabilities of this approach and its potential impact in flood risk management activities the real flood event occurred on the River Secchia (Italy) on January 2014 as a consequence of a breach in the river right embankment, was simulated. The levee breach was in all probability triggered by the presence of a burrowing animal den. The region of Northern Italy under investigation, bounded by the Po River and by its two consecutive tributaries Secchia and Panaro, was in the past subject to several floods due to breach collapse. At least three of these events were catastrophic and caused the inundation of wide plains (more than 500 km^2), with considerable water depths (6-7 m) (Aureli and Mignosa, 2004). If the breaching mechanisms of the past events are only partially known, in the recent years the awareness of the causes of levee collapses is progressively increasing. Among the most important causes of levee breaching are nowadays included the dens of burrowing animals whose presence in the levee body can represent a real threat capable to trigger the erosion processes.

A lot of research is currently being undertaken to achieve a realistic representation of the failure mechanisms of earthen dams and levees. Many studies (Zhu et al., 2004, Macchione, 2008, Macchione and Rino, 2008) describe the characteristics of dam breaches by estimating various parameters: geometrical (height, width, failure time), hydraulic (reservoir volume, initial water height), geotechnical (material erodibility). Recently Viero et al. (2013) proposed the reconstruction of different flooding events due to levee breaches in Northern Italy considering both overtopping and piping processes, on the basis of a simplified physically based 1D-link capable to simulate the breach initiation and growth In the present study, the breach evolution in time has been modelled according to the field data collected during the event.

Model calibration was achieved against the high amount of field data collected during the event, not least the radar data available from the COSMO-SkyMed archive and captured about 60 hours after the beginning of the levee collapse.

The paper is organized as follows: in Section 1, the study case and a collection of the available field data are presented. Section 2 is dedicated to the description of the numerical simulations; the model is briefly illustrated and detailed analyses regarding the topographic data, the roughness estimation and the imposed boundary conditions are reported. The simulation results are shown and verified in Section 3 and finally, in Section 4 the conclusions of the work are reported.

1. Study area and available field data

At 6:00 A.M., during the flood event of January 19th 2014, a levee breach occurred in the Secchia right bank near Modena (North-Central Italy, Figure 1). Here the river is bounded by artificial earthen levees of remarkable height above the surrounding lands. Even if water levels in the river were far from overtopping the crest, a small portion of the levee body collapsed, triggering the flooding. The breach was in all likelihood originated by the presence of burrowing animals dens, as inferred *a posteriori* by an accurate inspection of high-resolution aerial photographs taken before the failure and by an incipient similar breach observed in the same day along the left levee of the neighbor Panaro River. Progressively the breach widened and deepened, reaching a maximum width of about 80 m at about 3:00 P.M. of January 19th 2014. The flooding caused the displacement of thousands of people and one death, 75 km^2 of flooded lands, and estimated overall losses for about 400 million euros. The information about timing, geometry and evolution of the levee breach were provided through direct observation and aerial photos (Figure 2).

Field information about flood propagation time and flooding extent, useful for calibration purposes, were achieved through press services, media and people directly involved or interested in the event.

Satellite synthetic Aperture Radar (SAR) observations, acquired at 3 m spatial resolution during the flooding event, were also obtained from the COSMO-SkyMed Mission archive and allowed a synoptic view of the flooding extent about 60 hours after the beginning of the breaching process.

2. Numerical simulations

2.1. Topographic data

The area involved by the flooding is characterized by the presence of two main villages and it is bounded at east by the left levee of the Panaro River, the right tributary of the Po River following the Secchia River.

A digital terrain model (1 m resolution), based on a LIDAR survey, was available to describe the geometry of the riverbeds and of the flooded area. Since the acquisition was performed during summer, when the Secchia river is almost totally dried up, no other information was necessary to correctly describe the bathymetry.

Many embankments of roads, railways and artificial channels cross the region and exerted an important influence on the flooding dynamics. To achieve a correct description of all these important geometrical features, a high resolution mesh is required in the mathematical modelling. To reach a good compromise between an accurate description of all the main characteristics of the bathymetry and the computational time, in the present study a Cartesian mesh with size equal to 5 m was adopted. In order to preserve the crest elevation of the artificial embankments after the downsampling of the DTM, each 5x5 m cell crossed by an embankment was identified and its elevation was set equal to the maximum value of the original 25 points belonging to that cell.

In Figure 3 a detail of the terrain elevation of a complex highway junction is shown, considering both the original DTM with 1 m resolution and the corrected 5 m resolution mesh adopted for the numerical modelling. The 5 m mesh is still capable to describe the details of all the embankments and highway ramps that may exert an influence on the flooding evolution.

2.2. Numerical model

The numerical model here adopted solves in a finite volume framework the integral form of 2D SWE (e.g. Toro 1999a):

$$\frac{d}{dt}\int_A \mathbf{U}\ dA + \int_C \mathbf{H}\cdot\mathbf{n}\ dC = \int_A \left(\mathbf{S}_0 + \mathbf{S}_f\right) dA. \qquad (1)$$

where A is the area of the integration element, C the element boundary, $\mathbf{n}$ the outward unit vector normal to C, $\mathbf{U}$ the vector of the conserved variables and $\mathbf{H} = (\mathbf{F},\mathbf{G})$ the tensor of fluxes in the x and y directions respectively:

$$\mathbf{U} = \begin{bmatrix} h \\ uh \\ vh \end{bmatrix}, \mathbf{F} = \begin{bmatrix} uh \\ u^2 h + \frac{1}{2} g h^2 \\ uvh \end{bmatrix}, \mathbf{G} = \begin{bmatrix} vh \\ uvh \\ v^2 h + \frac{1}{2} g h^2 \end{bmatrix}, \tag{2}$$

where h is the flow depth, u and v are the velocity components in the x and y directions and g is the acceleration due to gravity. The bed and friction slope source terms $\mathbf{S}_0$ and $\mathbf{S}_f$ are expressed according to the following relations:

$$\mathbf{S}_0 = \left[0; -gh\frac{\partial z}{\partial x}; -gh\frac{\partial z}{\partial y} \right]^T$$
$$\mathbf{S}_f = \left[0; -gh\frac{n_f^2 u\sqrt{u^2+v^2}}{h^{4/3}}; -gh\frac{n_f^2 v\sqrt{u^2+v^2}}{h^{4/3}} \right]^T \tag{3}$$

in which z is the bed elevation with respect to a horizontal reference plane and n_f is the roughness coefficient according to the Manning equation. For the friction source term the implicit discretization of Caleffi et al. (2003) is adopted: this prevents the formation of spurious oscillations in the presence of very small depths, which might occur when a naive explicit formulation is used, whereas an explicit discretization of the bed slope is performed in order to satisfy the C-property also in presence of wet-dry interfaces (Vacondio et al. 2014). The problem of obtaining a balance between fluxes and source terms in Equation (1) has received considerable attention in the recent literature. Some authors addressed the problem rectifying the SWEs formulation by numerical treatment (Vázquez-Cendón, 1999, Zhou et al., 2001; Valiani & Begnudelli, 2006a,b and Aureli et al., 2008;). Mourillo & García-Navarro (2010, 2012) introduced a new approach defining a weak solution that inherently incorporates the source terms. Rogers et al. (2003) derived an algebraic modification of Equation (1) capable to balance the hyperbolic system of equations, regardless of the discretization of the slope source term and of the approximate Riemann solver. Liang & Borthwick (2009) further modified the idea presented by Rogers et al. (2003), by proposing a different way to manipulate the SWEs, which is suitable also for problems with wet-dry interfaces.

In this work the Liang & Borthwick (2009) formulation is adopted and the terms of Equations (2) are modified as follows:

$$\mathbf{U} = [\eta;\ uh;\ vh]^T$$
$$\mathbf{F} = \begin{bmatrix} uh \\ u^2h + \tfrac{1}{2}g\left(\eta^2 - 2\eta z\right) \\ uvh \end{bmatrix},\ \mathbf{G} = \begin{bmatrix} vh \\ uvh \\ v^2h + \tfrac{1}{2}g\left(\eta^2 - 2\eta z\right) \end{bmatrix}, \qquad (4)$$

where $\eta = h + z$ is the free surface elevation above datum and the bottom source term $\mathbf{S}_0$ is:

$$\mathbf{S}_0 = \left[0;\ -g\eta\frac{\partial z}{\partial x};\ -g\eta\frac{\partial z}{\partial y} \right]^T \qquad (5)$$

The bottom source term is discretized using a centered formulation. As indicated before the C-property is inherently guaranteed by the modified form of the SWEs reported in Equation (4).

The partial differential equations (1) are solved on a Cartesian grid adopting a second order accurate (in space and time) Finite Volume (FV) numerical approximation of the SWEs. Regardless of the order of accuracy, the fluxes are calculated using a HLLC approximate Riemann solver (Toro, 1999b).

The fluxes **F** and **G** in x and y directions are evaluated at the intercells (i ± ½) and (j ± ½), respectively. To avoid the formation of high velocities and instabilities, if the water depth $h_{i,j}$ is lower than a very small threshold h_ε the cell is dried (h = 0). To prevent any significant mass conservation error h_ε has been defined equal to 1×10^{-5}, which is close to the machine precision. Moreover in the cells with water depth smaller than 20 cm the fluxes are corrected as suggested by Kurganov & Petrova (2007). In this way the development of non-physical velocities close to the wet dry front is avoided.

The second order of accuracy in time is obtained by a second order Runge-Kutta method:

$$\mathbf{U}_{i,j}^{n+1} = \mathbf{U}_{i,j}^{n} + 0.5\Delta t^n \left[\mathbf{D}_i\left(\mathbf{U}_{i,j}^{n}\right) + \mathbf{D}_i\left(\mathbf{U}_{i,j}^{n+\frac{1}{2}}\right) \right] \qquad (6)$$

where the superscript n represents the time level, the subscripts i, j and Δx, Δy are the cell positions and the grid sizes in x and y directions, respectively, and Δt^n is the timestep calculated accordingly to the Courant–Friedrichs-Lewy condition. The operator $\mathbf{D}_i(\mathbf{U}_{i,j})$ is defined as:

$$\mathbf{D}_i\left(\mathbf{U}_{i,j}\right) = -\frac{\left(\mathbf{F}_{i+\frac{1}{2},j} - \mathbf{F}_{i-\frac{1}{2},j}\right)}{\Delta x} - \frac{\left(\mathbf{G}_{i,j+\frac{1}{2}} - \mathbf{G}_{i,j-\frac{1}{2}}\right)}{\Delta y} + \mathbf{S}_0 + \mathbf{S}_f \quad (7)$$

and $\mathbf{U}_{i,j}^{n+1/2}$ is obtained as:

$$\mathbf{U}_{i,j}^{n+\frac{1}{2}} = \mathbf{U}_{i,j}^{n} + \Delta t^n \mathbf{D}_i\left(\mathbf{U}_{i,j}\right) \quad (8)$$

The modeling of a parallel system based on a GPU architecture requires some adaptation of traditional sequential algorithms.

The update of the conservative variables (vector $\mathbf{U}$) in a single time step from time t^n to time $t^{n+1} = t^n + \Delta t$, is described by a sequence of eight sub tasks (Vacondio et al. 2014). The CPU controls the iteration evolution and invokes the various tasks in order. Each task can be processed in parallel and is described by a distinct CUDA kernel.

Several optimization procedures have been developed, including a novel and efficient Block Deactivation Optimization (BDO), the implicit local ghost approach for the assignment of boundary conditions and a careful implementation to reduce the information exchanges between CPU and GPU. The code was validated against many severe benchmark test cases (Vacondio et al., 2014). The parallel implementation allows excellent speedup with respect to the number of processors in the GPU.

2.3. Riverbed roughness estimation

In the considered reach, only few discontinuous floodplains of relatively small extent are present between the river levees. This suggested to characterize the river region by means of a unique roughness coefficient. For the Secchia River a 1D hydraulic model calibrated on the basis of four historical level gauges located along the river reach (the two most upstream being Ponte Alto and Ponte Bacchello) was developed in the past and thus available. Moreover, for the mentioned gauging stations, stage-discharge relationships are still published and updated by ARPA (Regional Agency for Environmental Protection in the Emilia-Romagna region), on the basis of regular discharge measures. However the roughness coefficient is sensitive both to model schematization (1D / 2D) and discretization (mesh size). Since in the present study a fully 2D model was adopted also for the riverbed, a new ad-hoc calibration was performed. With this aim the most significant and well documented event occurred in the last ten years (23rd - 30th December 2009) was adopted. In Figure 4 the discharge hydrograph at Ponte Alto (converted from the recorded levels through the station stage-discharge relationship) and the stage hydrograph at Ponte Bacchello, imposed as upstream and downstream boundary conditions respectively, are shown.

To estimate the most suitable roughness coefficient the Nash-Sutcliffe efficiency criterion (Nash and Sutcliffe, 1970), E_h, was adopted with reference to the water levels at Ponte Alto gauging station:

$$E_h = \left[1 - \frac{\sum_{i=1}^{N}\left(h_i^{act} - h_i^{est}\right)^2}{\sum_{i=1}^{N}\left(h_i^{act} - \overline{h}^{act}\right)^2}\right] \cdot 100 \qquad (9)$$

where N is the total number of stage hydrograph data, h_i^{act} and h_i^{est} are the i-th observed and estimated water level values respectively, and $\overline{h}^{act}$ is the mean value of the actual hydrograph.

Table 1 shows the values of E_h for n_f = 0.067, 0.05 and 0.03 $m^{-1/3} \cdot s$ and Figure 5 shows the comparison between computed and observed water levels at Ponte Alto. Water levels computed with n_f = 0.05 $m^{-1/3}s$ showed the best agreement with the registered data and this value of Manning roughness coefficient was therefore adopted to characterize the riverbed.

2.4. Evaluation of the inflow boundary condition

The inflow discharge for the event of January 2014 (upstream boundary condition) was firstly obtained by simply converting the stage hydrograph recorded at Ponte Alto gauging station with the available stage-discharge relationship. However this rating curve was expected to underestimate the inflow discharges after the occurrence of the breach, which is located only 6 km downstream of the gauging station itself. The comparison between registered and simulated water elevation obtained in this way is shown in Figure 6. The agreement is very satisfactory before the breach formation, whereas afterwards the computed water elevations systematically underestimate the registered ones. This confirms that the breach gives origin to a drawdown profile capable to exert a significant influence on the rating curve at Ponte Alto.

In order to assess this problem, the 2D numerical model was run assuming a synthetic triangular flood wave as upstream boundary condition and match wellin presence of the fully developed breach. The stage-discharge values, obtained from this numerical simulation at Ponte Alto, were fitted by a power law function to obtain a new rating curve for the station. This rating curve was then adopted to convert water elevations into discharges for the January 2014 event only after the complete development of the breach, whereas the original stage-discharge relationship was used before the beginning of the breach formation. During the breach evolution (between 6.00 AM and 3.00 PM of the 19th January 2014) a linear interpolation between the two hydrographs was adopted in order to take into account the progressive opening of the breach. The new hydrograph is plotted, together with the uncorrected one, in Figure 7: after the opening of the breach the modified discharges are significantly greater, with an increase in the peak value of about 80 m^3/s.

The water levels at Ponte Alto, obtained imposing the new discharge hydrograph, are also plotted in Figure 6. The numerical results with the corrected inflow boundary condition are in excellent agreement with the registered data, and the issue of underestimation of water levels after the breach formation is addressed.

2.5. Flooded area roughness estimation

Calibration of the roughness values in the flooded area outside the river region was accomplished in two steps with the aim of evaluating two different Manning's *n* values suitable to represent the roughness of rural and urban areas, respectively. With regard to the rural areas, the adoption of a unique roughness coefficient was fairly justified by the almost homogeneous land use characterizing the cropland in the low plain near Modena. Urban areas were then considered as regions of higher resistance, characterized by their specific Manning coefficient to be estimated afterwards the calibration of the roughness coefficient of the rural areas. Different methodologies, alternative to the adopted approach, are available in literature to account for the influence of the buildings on the flooding dynamics (Soares-Frazão et al., 2008; Schubert et al., 2008; Schubert and Sanders, 2012); anyway a detailed modeling of the flood propagation through the buildings was beyond the scope of the present study.

The first calibration step, devoted to the evaluation of the resistance parameter for the rural areas, outside the riverbed, was accomplished holding the in-channel roughness at 0.05 $m^{-1/3}\cdot s$ and executing three different runs each characterized by a different uniform value of n_f, respectively equal to 0.07, 0.05 and 0.03 $m^{-1/3}\cdot s$. For each simulation the time of arrival of the flooding at the south-western boundary of the Bastiglia urban area, occurred actually 6.75 hours after the beginning of the breaching process, was evaluated. Figure 8 shows the maps of the flooding extent at 0:45 PM on 19th January 2014 for the three mentioned simulations. The time of the comparison was chosen properly to guarantee that the flood propagation did not interest yet any urban area.

Incidentally, the roughness value $n_f = 0.05$ $m^{-1/3}s$ allows again to correctly reproduce the arrival time of the wetting front at the entrance of the urban area of Bastiglia, while the arrival is anticipated and delayed of about half an hour adopting in the model the lower (0.03) and the higher

(0.07) roughness coefficients, respectively. The obtained results show that the flooding dynamics is not dramatically sensitive to the variation of the resistance parameter assigned to the rural areas. Additional numerical simulations were then performed holding the rural areas roughness at 0.05 $m^{-1/3}\cdot s$ and varying the urban areas resistance parameter to reproduce the overall effect of buildings. The calibration was accomplished on the basis of a correct reproduction of the arrival time of the flooding at Bomporto. Five different values of n_f, equal to 0.083, 0.111, 0.143, 0.2 and 0.5 $m^{-1/3}\cdot s$, were assumed. The Manning roughness value $n_f = 0.143$ $m^{-1/3}\cdot s$ allows to correctly reproduce the arrival of the flood front at Bomporto, while the flood arrival is anticipated of 2.75 and 1 hours considering n_f equal to 0.5 and 0.2 $m^{-1/3}\cdot s$ respectively, and it is delayed of 1.5 and 4.5 hours considering n_f equal to 0.083 and 0.111 $m^{-1/3}\cdot s$, respectively. Unlike the roughness of the rural area, the flooding arrival time at Bomporto is significantly influenced by the roughness coefficient assumed to describe the urban area at Bastiglia. On the contrary, numerical results are not as sensitive to the roughness coefficient assumed to describe the Bomporto urban area, since there the velocities almost vanish, due to the presence of the river embankments of Panaro River and Naviglio channel which surround the village (see the following Figure 9).

A further validation of the quality of the calibration was provided by the information about the volume of water lifted by the pumping station of Santa Bianca (about 18 Mm^3) that is in good agreement with the computed value of the volume flowed in the northern portion of the flooded domain (about 17.5 Mm^3).

3. Simulations and results

The flooding event was simulated from 12:00 PM of January 17th 2014, when the registered water levels at the gauging stations started to increase significantly, till 6.00 AM of January 21th 2014 when the flood event might be considered as concluded (see Figure 10). According to field observations the breach was assumed to progressively evolve during a period of 9 hours reaching a maximum width of about 80 m.

The 2D simulations entailed a storage of about 2671 MB on the graphic card using 7.2 million computing cells and required about 6 computing hours to simulate the period from 12:00 PM of January 17th 2014 till 6.00 AM of January 21th 2014 (90 hours).

3.1. River reach

Figure 10 shows the flow hydrographs computed at the breach section and in other two sections along the river reach, respectively 200 m upstream and downstream of it. At the end of the breach evolution process about 525 m^3/s, which correspond to more than 87% of the upstream discharge, are flowing through the breach, whereas only the remaining 13% proceed downstream.

Figure 11 shows the stage hydrograph close to the breach. Here the spatial variability of the water stage is high, due to the drawdown effect exerted by the outflowing discharge, so the figure is just indicative. After the beginning of the breaching process (about 6:00 A.M. of January 19th) water levels still increase, reaching the highest value of 36.05 m a.s.l. around 8:00 A.M. Then the levels start to decrease quite abruptly reaching the value of about 33 m a.s.l. in the following 7 hours. After the stabilization of the breach opening the water stages continue to decrease, with a further lowering of 2 meters in about 33 hours.

3.2. Flooded area

In Figure 12 some significant frames of the flooding evolution are reported. According to the available observations collected during the event, the timing of the simulated inundation is in good agreement with the real flood event evolution. About 1 hour after the levee breach (7.00 A.M. of 19th January 2014), water quickly flooded near lowlands in North-East direction (Figure 12-a). At

2.00 P.M. the flood wave reached the center of the urban area of Bastiglia (Figure 12-b), where most people were already evacuated. Few hours later (9.00 P.M.), the countryside of Sorbara was flooded (Figure 12-c). At 10:30 A.M. of 20th January 2014, water reached the central Matteotti square in Bomporto (Figure 12-d). At 2:00 P.M. of 20th January 2014 the flood wave reached the SP5 road near Camposanto (Figure 12-e) which was overtopped only about 4 hours later (6:00 P.M. of 20th January 2014) (Figure 12-f).

In the numerical simulation the overall volume flowed out from the breach was estimated to be around 39 Mm^3. About 21.5 Mm^3 of this overtopped the levees of the Naviglio channel at Bastiglia and moved to the eastern areas up to Bomporto, whereas about 17.5 Mm^3 went ahead and flooded the northern portion of the domain.

Figure 13 shows the comparison between real flooded areas, spotted through aerial images, and computed ones. The first pair shows that the flooding is correctly reproduced by the computations at Bomporto, where the East portion is flooded while the West one is not. The second pair of images shows that the influence of the disused railway embankment, located north-east of Bastiglia, and the flooding of the surrounding cultivated lands are also correctly represented by the numerical model.

Comparison between numerical results and SAR data was also performed. The COSMO-SkyMed 4 satellite crossed the areas of Modena on the 21th January 2014, acquiring an image at 5:20 P.M., at a high spatial resolution of 3 m.

Figure 14 compares the extent of the flooded region deduced from the SAR image with that obtained through the numerical computations. Due to the satellite flight path, the extreme North-East portion of the domain under investigation was not covered by the image frame. The inundation extent is well enough captured by the numerical model, especially in the south and north west ends. Despite the high-resolution information of the flood extent available in the SAR image, in a not negligible number of land parcels, located at the edge of the flooded area, the image is biased due to multiple reflections between the water and the emerging vegetation which causes an increased backscatter compared to that from a smooth open water surface (Mason et al. 2012a, Mason et al. 2012b). This is confirmed by the available aerial views captured during the event, one of which is shown in Figure 15. Flooded land parcels, characterized by low backscatter, are apparently contiguous to increased backscatter areas, which would be considered as dry on the basis of direct analysis of the SAR image only. This issue makes impossible the evaluation of quantitative metrics, like the one proposed by Bates and De Roo (2000), to measure the capability of the numerical model to reproduce the observed inundation extent. However, the availability of aerial photos of the parcels of land of doubtful characterization confirms unequivocally that the extent of the inundation is correctly reproduced by the numerical simulations.

Figure 16 shows the map of maximum water depths (envelope) obtained by the numerical model. Apart from the river and channel beds, the maximum values occur in the southern portion of the flooded region, where water depths raise up to 2.6-2.8 m, due to the blocking effect of the several embankments crossing this area. These values, especially in the urban areas where the signs of the flood are more reliable due to the presence of mud, are in very good agreement with the observations. Smaller depths (0-1 m) were computed (and observed) in the northern portion of the flooded region, with the exception of the area just upstream the SP5 road near Camposanto, where maximum depths of 1.4-1.6 m were computed, due to the retaining effect of the road embankment.

Finally, Figure 17 shows the map of the computed arrival times of the flooding. Very different arrival times at a short distance highlight the blocking/delaying effects exerted on the flooding dynamics by the embankments of artificial channels, roads and railways. As an example, points A and B, located 1 km apart but on two opposite sides of a channel embankment, are reached by the flooding 10.5 and 24.5 hours after the levee failure, respectively. Some areas in the most southern part of the domain, where the ground elevation is higher, were flooded by backwater effects only 40-45 hours after the levee collapse (blue colors). From the map it is also evident the long delay (more than 24 hours, green colors) occurred between the breach triggering and the flooding of Bomporto. This suggests that some countermeasures (sandbags, inflatable rubber dams, etc.) could have been implemented during the event in order to avoid the flooding or reduce the water depths in this urban area.

4. Discussion and conclusions

Flood management in wide lowlands crossed by rivers bounded by artificial earthen levees of remarkable height, as occurs in the Po River valley, is a crucial issue for multiple reasons. On one side the trend in flood frequency appears to be increasing with a continue worsening of the stress exerted upon the embankments, moreover the huge length makes very difficult the maintenance of the defense systems in perfect working order; take for example the problem represented by the presence of burrowing animals, whose deep dens may be the root cause of the significant piping problems threatening the structural integrity of the levees. This was confirmed by the real event investigated here, during which the Secchia and Panaro embankments were both subject to break processes triggered by the presence of dens, despite of an hydrologic input of low return period. On the other side it has to be considered that the domain is a portion of the main wide plain area of the southern Europe which is rich in history and highly productive. Due to the value of the elements exposed to risk, inundations of small extent lead often to economic losses of hundreds of million euros . For the event here considered the flooding caused the displacement of thousands of people, one death, 75 km^2 of flooded lands, and estimated overall economic losses for about 400 million euros (more than 5 M€/km^2). The development and application of tools capable to provide accurate and fast predictions for flood management in these territories is therefore crucial capital and the open challenge is the development of real time flood modelling tools capable to provide help in the definition of protection strategies during the flood events.

In order to setup real-time flooding-forecast systems, useful for flood risk management, the time of simulation is certainly a main issue. With the aim of real-time flood protection, as a matter of fact, the computational time proper of traditional serial 2D shallow-water numerical models is still excessive and makes their adoption impossible. The new parallel code here presented implemented on CUDA-enabled GPU cards seem to fit for the purpose, allowing a high spatial resolution and achieving a ratio between physical time and runtime greater than 15 (about 6 computing hours are necessary to simulate 90 hours of physical time).

The continuously increasing storage capabilities of commercially available graphic cards permits the adoption of grids composed of several millions computing cells, with the possibility to describe the domain geometry at high resolution. In this way the LiDAR 1 m DTMs, which are now becoming increasingly widespread, can be adopted with a minimum degrading, without appreciable loss of accuracy in the representation of all the geometrical elements that can exert a significant influence on the flood propagation. The exponential growth of all the related technologies, at the affordable cost of standard desktop computers, makes the GPU parallelization an attractive modelling approach. In confirmation of this fast growing process a new CUDA-GPU card, that halves the computational time of the one here adopted, has been in the news recently. The original GPU-parallelized model adopted here allowed an integrated description of the river and the flood prone areas in a unique computational domain; the flow phenomenon was then modelled in its entirety, avoiding the special treatments required at the linking of 1D / 2D numerical schemes. This feature, along with the small time scale ratio characterizing the computations, suggests that a database of a high number of possible flooding scenarios due to levee collapse, also under different hydrologic inputs, could be set up for a region of interest within a very reasonable computational time and cost, inconceivable just a few years ago.

The riverbed roughness has been calibrated using the available data at Ponte Alto gauging station for the most significant previous flooding event in which the low lying area outside the river region was not flooded. Conversely for the flooded areas two different roughness coefficients have been defined for the rural and urban areas, respectively. Those coefficients have been adjusted in such a way that the numerical simulation can reproduce the arrival times of the floodings at different locations.

For an occurrence of a levee collapse the ‘offline’ adoption of the model, thanks to the availability of the result database, would provide decision-makers with a valuable tool for the implementation of mitigation strategies, allowing to infer with a reasonable confidence the flooding event evolution with respect to the more similar scenario already simulated. Again with the aim of implementing flood event management strategies, civil protection activities could take a great advantage also of the coupling of the GPU-parallelized tool here presented with weather forecast and rainfall-runoff models, thus allowing an ‘online’ model application during an event. In this case the uncertainty in the computed flood extents, due to the absence of prior calibration, could be reduced through data assimilation combining the flow variables with observations. Spatially distributed information about inundation extents can be achieved through satellite high-resolution SAR images that are characterized by a unique all-weather day-night capability. However, as presented here due to the high amount of different kinds of field observations, proper image segmentation algorithms have to be implemented to estimate correct waterline levels and positions due to the increased backscatter induced by the emergent vegetation that gives origin to an underestimation of the flood extents in some inundated parcels.

In the particular case here considered and discussed, both ‘offline’ and ‘online’ applications of the presented modelling tool would have been of help to the devising of emergency protection measures. This is especially true with respect to those territories that, for the relative distance from the breach site, would have been involved by the flooding many hours after the levee collapse. The knowledge of the inundation propagation characteristics, even in the presence of the many sources of uncertainty usually affecting the hydrological scenarios, would have more effectively allowed the adoption of emergency mitigation measures with the aim of avoiding the inundation or at least reducing the water depths in the built up areas and the consequent human and economic losses.

Acknowledgments

Interregional Agency for the Po River (AIPo) and personnel directly involved in the management of the emergency are gratefully acknowledged for providing a large amount of field data and observations. We acknowledge the CINECA Award P-FLOOD2-HP10CHAL0S, 2014 under the ISCRA initiative for the availability of high performance computing resources and support. Luigi Romenghi is gratefully acknowledged for shooting and providing the aerial views of the flooding.

References

Aureli, F., Mignosa, P., 2004. Flooding scenarios due to levee breaking in the Po river. Proceedings of the ICE - Water Management, Volume 157, Issue 1, 01 March 2004.

Aureli, F., Mignosa, P., Ziveri, C., Maranzoni, A., 2006. Fully-2D and quasi-2D modeling of flooding scenarios due to embankment failure. International Conference on Fluvial Hydraulics - River Flow 2006; Lisbon; Portugal; 6 September 2006 through 8 September 2006.

Aureli, F., Maranzoni, A., Mignosa, P., Ziveri, C., 2008. A weighted surface-depth gradient method for the numerical integration of the 2d shallow water equations with topography. Adv. Water Resour. 31, 962-974.

Bates, P., De Roo, A.P.J., 2000. A simple raster-based model for flood inundation simulation. Journal of Hydrology, 236, 54-77.

Bladé, E., Gómez-Valentin, M., Dolz, J., Aragón-Hernández, J.L., Corestein, G., Sánchez-Juny, M. 2012. Integration of 1D and 2D finite volume schemes for computations of water flow in natural channels, Adv Water Resourc, 42, 17–29

Brodtkorb, A.R., Saetra, M.L. Altinakar, M., 2012. Efficient shallow water simulations on GPUs: implementation, visualization, verification, and validation. Comput. Fluids, 55 1–12.

Caleffi, V., Valiani, A., Zanni, A., 2003. Finite volume method for simulating extreme flood events in natural channels. J. Hydraul. Res. 41, 167-177.

Crossley A, Lamb R, Waller S. 2010. Fast solution of the Shallow Water Equations using GPU technology, Proceedings of the British Hydrological Society 3rd International Symposium, Newcastle, UK, 13–19 July 2010

De la Asunción, M., Castro, M.J., Fernández-Nieto, E., Mantas, J.M., Acosta, S.O. , González-Vida J.M., 2013. Efficient GPU implementation of a two waves TVD-WAF method for the two-dimensional one layer shallow water system on structured meshes Comput. Fluids, 80 (2013), pp. 441–452

Di Baldassarre, G., Castellarin, A., Brath, A., 2009. Analysis of the effects of levee heightening on flood propagation: example of the River Po, Italy. Hydrological Sciences Journal 54:6, 1007-1017.

Di Baldassarre, G., Uhlenbrook, S., 2012. Is the current flood of data enough? A treatise on research needs for the improvement of flood modelling. Hydrol. Process., 26: 153–158. doi: 10.1002/hyp.8226.

Domeneghetti, A., Vorogushyn, S., Castellarin, A., Merz, B., Brath, A., 2013. Probabilistic flood hazard mapping: Effects of uncertain boundary conditions. Hydrology and Earth System Sciences, Volume 17, Issue 8, Pages 3127-3140.

Dottori, F., Di Baldassarre, G., Todini, E., 2013. Detailed data is welcome, but with a pinch of salt: Accuracy, precision, and uncertainty in flood inundation modeling. Water Resour. Res., 49, 6079–6085, doi:10.1002/wrcr.20406.

Gallegos, H.A., Schubert, J.E., Sanders, B.F., 2009. Two-dimensional, high-resolution modeling of urban dam-break flooding: A case study of Baldwin Hills, California. Advances in Water Resources, Volume 32, Issue 8, August 2009, Pages 1323-1335, ISSN 0309-1708, http://dx.doi.org/10.1016/j.advwatres.2009.05.008.

Hallegatte, S., Green, C., Nicholls, R.J., Corfee-Morlot, J., 2013. Future flood losses in major coastal cities, Nature Climate Change 3,802–806.

Horritt, M.S., Bates, P.D., 2002. Evaluation of 1D and 2D numerical models for predicting river flood inundation, Journal of Hydrology 268, 87-99, Issues 1–4.

Kurganov, K., Petrova, G., 2007. A second-order well-balanced positivity preserving central-upwind scheme for the Saint-Venant system, Communications in Mathematical Sciences 5(1), 133–160.

I.Yu. Gejadze, J. Monnier, 2007. On a 2D ’zoom’ for the 1D shallow water model: coupling and data assimilation, Comput Methods Appl Mech Eng, 196, 4628–4643.

Jongman, B., Hochrainer-Stigler, S., Feyen, L., Aerts, J.C.J.H., Mechler, R., Botzen, W.J.W., Bouwer, L.M., Pflug, G., Rojas, R., Ward, P.J., 2014. Increasing stress on disaster-risk finance due to large floods, Nature Climate Change 4,264-268.

Lacasta, A., Morales-Hernández, M., Murillo, J., García-Navarro, P., 2014. An optimized GPU implementation of a 2D free surface simulation model on unstructured meshes, Advances in Engineering Software, 78, 1-15, http://dx.doi.org/10.1016/j.advengsoft.2014.08.007

Lacasta, A., Juez, C., Murillo, J., García-Navarro, P., 2015. An efficient solution for hazardous geophysical flows simulation using GPUs, Computers & Geosciences, 78, 63-72, http://dx.doi.org/10.1016/j.cageo.2015.02.010.

Leskens, G., Brugnach, M., Hoekstra, A.Y., Schuurmans, W., 2014. Why are decisions in flood disaster management so poorly supported by information from flood models?, Environmental Modelling and Software 53, 53-61.

Liang, Q., Borthwick, A.G.L., 2009. Adaptive quadtree simulation of shallow flows with wet-dry fronts over complex topography. Comput. Fluids 38, 221-234.

Macchione, F., 2008. Model for Predicting Floods due to Earthen Dam Breaching. I: Formulation and Evaluation. J. Hydraul. Eng. 134: 1688-1696.

Macchione, F. and Rino, A., 2008. Model for Predicting Floods due to Earthen Dam Breaching. II: Comparison with Other Methods and Predictive Use. J. Hydraul. Eng. 134: 1697-1707.

Marks, K., Bates, P., 2000. Integration of high-resolution topographic data with floodplain flow models. Hydrol. Process., 14: 2109–2122. doi: 10.1002/1099-1085.

Masoero, A., Claps, P., Asselman, N. E. M., Mosselman, E., Di Baldassarre, G., 2013. Reconstruction and analysis of the Po River inundation of 1951. Hydrol. Process. 27, 1341-1348.

Mason, D.C., Schumann, G.J.P., Neal, J.C., Garcia-Pintado, J., Bates, P.D., 2012a. Automatic near real-time selection of flood water levels from high resolution Synthetic Aperture Radar images for assimilation into hydraulic models: A case study. Remote Sensing of Environment. Volume 124. Pages: 705-716.

Mason, D.C., Davenport, I. J., Neal, J.C., Schumann, G.J.P., Bates, P.D., 2012b. Near Real-Time Flood Detection in Urban and Rural Ares Using High-Resolution Synthetic Aperture Radar Images. IEEE Transactions on Geoscience and Remote Sensing, Vol. 50, N°8, August 2012. Pages 3041-3052.

Mazzoleni, M., Bacchi, B., Barontini, S., Di Baldassarre, G., Pilotti, M., Ranzi, R., 2014. Flooding Hazard Mapping in Floodplain Areas Affected by Piping Breaches in the Po River, Italy. J. Hydrol. Eng., 19(4), 717–731.

Morales-Hernández, M., García-Navarro, P., Burguete, J., Brufau, P., 2013. A conservative strategy to couple 1D and 2D models for shallow water flow simulation. Computers & Fluids, 81, 26-44.

Morales-Hernández, M., Lacasta, A., Murillo, J., Brufau, P., García-Navarro, P., 2014. A Comparative study of accuracy and performance between a fully 2D GPU based and a 1D-2D coupled numerical model in a real river. Proceedings of International Conference on Hydrodinformatics, HIC , 2014, New York City, USA.

Murillo, J., García-Navarro, P., 2010. Weak solutions for partial differential equations with source terms: Application to the shallow water equations. Journal of Computational Physics, 229(11), 4327-4368, doi: 10.1016/j.jcp.2010.02.016.

Murillo, J., García-Navarro, P., 2012. Augmented versions of the HLL and HLLC Riemann solvers including source terms in one and two dimensions for shallow flow applications, Journal of Computational Physics, 231(20), 6861-6906, 10.1016/j.jcp.2012.06.031.

Nash, J.E., Sutcliffe, J.V., 1970. River flow forecasting through conceptual models part I - A discussion of principles. J Hydrol 1970;10(3):282–90. http://dx.doi.org/10.1016/0022-1694(70)90255-6.

Rogers, B.D., Borthwick, A.G.L., Taylor, P.H., 2003. Mathematical balancing of flux gradient and source terms prior to using roes approximate Riemann solver. J. Comput. Phys. 192, 422-451.

Sanders, B.F., Schubert, J.E., Detwiler, R.L., 2010. Parbrezo: a parallel, unstructured grid, godunov-type, shallow-water code for high-resolution flood inundation modeling at the regional scale. Advances in Water Resources, Volume 33, Issue 12, December 2010, Pages 1456-1467, ISSN 0309-1708.

Schubert, J.E., Sanders, B.F., Smith, M.J., Wright, N.G., 2008. Unstructured mesh generation and landcover-based resistance for hydrodynamic modeling of urban flooding. Advances in Water Resources, 31 (12),1603-1621.Schubert, J.E., Sanders, B.F., 2012. Building treatments for urban flood inundation models and implications for predictive skill and modeling efficiency. Advances in Water Resources, 41, 49-64, doi: 10.1016/j.advwatres.2012.02.012.

Schumann, G.J.P., Bates, P.D., Neal, J.C., Andreadis, K.M., 2014. Fight floods on a global scale. Nature 507. 169.

Smith, L.S., Liang, Q., 2013. Towards a generalised GPU/CPU shallow-flow modelling tool. Computers & Fluids, 88, 334-343, doi: 10.1016/j.compfluid.2013.09.018.

Soares-Frazao, S., Lhomme, J., Guinot, V., Zech, Y., 2008. Two-dimensional shallow-water model with porosity for urban flood modelling. Journal of hydraulic research, Volume 46, Issue 1, Pages 45-64.

Toro, E., 1999a. Shock Capturing Methods for Free Surface Shallow Water Flows. Wiley, New York.

Toro, E., 1999b. Riemann Solvers and Numerical Methods for Fluid Dynamics. Springer.

Vacondio, R., Dal Palù, A., Mignosa, P., 2014. GPU-enhanced Finite Volume Shallow Water solver for fast flood simulations. Environ. Model. Softw. 57, 60-75.

Valiani, A., Begnudelli, L., 2006a. Divergence form for the bed slope source term in shallow water equations. ASCE J. Hydraul. Eng. 146, 652-665.

Valiani, A., Begnudelli, L., 2006b. Divergence form for bed slope source term in shallow water equations. J. Hydraul. Eng. 132, 652-665.

Vázquez-Cendón, M.E., 1999. Improved Treatment of Source Terms in Upwind Schemes for the Shallow Water Equations in Channels with Irregular Geometry, J. Comput. Phys., 148(2), 497-526,
Viero, D. P., D'Alpaos, A., Carniello, L., Defina, A., 2013. Mathematical modeling of flooding due to river bank failure. Adv. Water Resour. 59, 82-94.

Zhou, J., Causon, D., Mingham, C., Ingram, D., 2001. The surface gradient method for the treatment of source terms in the shallow-water equations. J. Comput. Phys. 168, 1-25.

Zhu, Y.H., Visser, P.J., Vrijling, J.K., 2004. Review on embankment dam breach modeling. Taylor and Francis Group, 1189-1196.

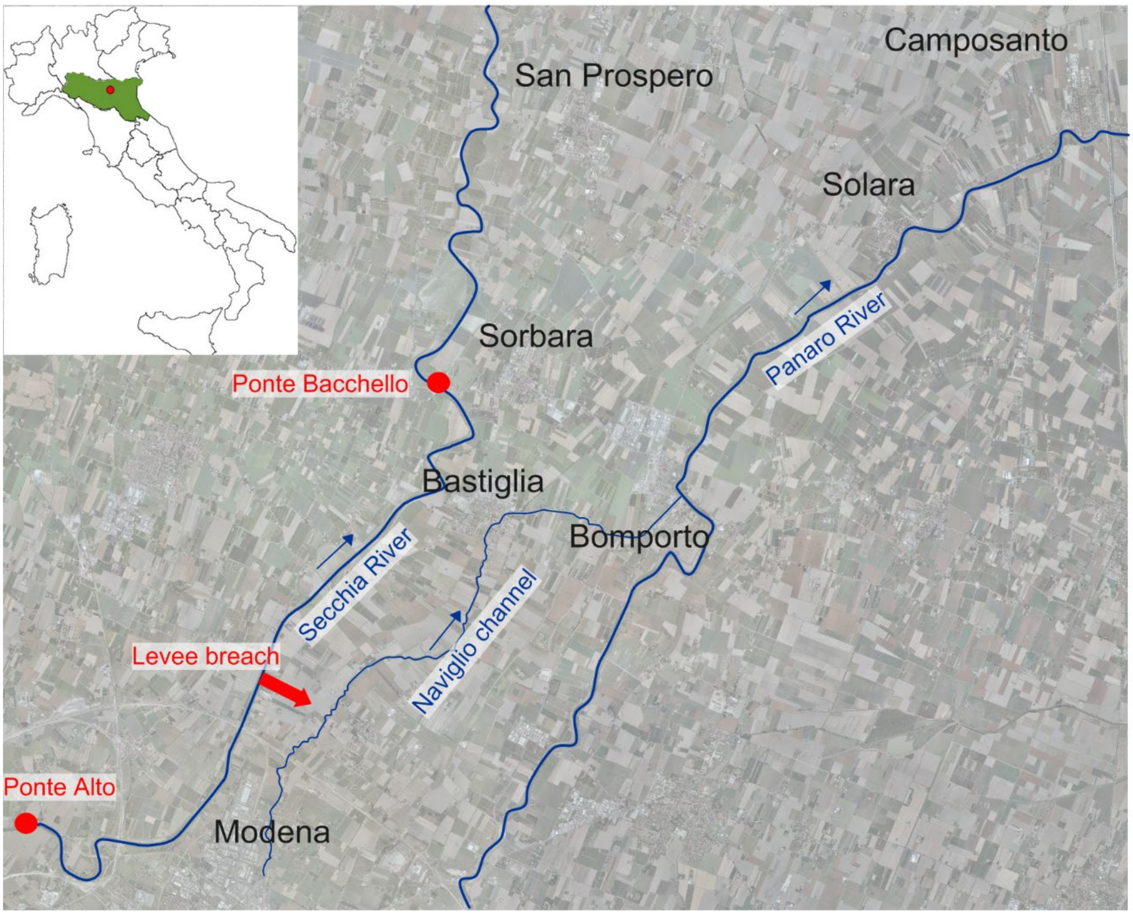
San Prospero
Camposanto
Solara
Sorbara
Panaro River
Ponte Bacchello
Bastiglia
Bomporto
Secchia River
Naviglio channel
Levee breach
Ponte Alto
Modena

 (a)	 (b)

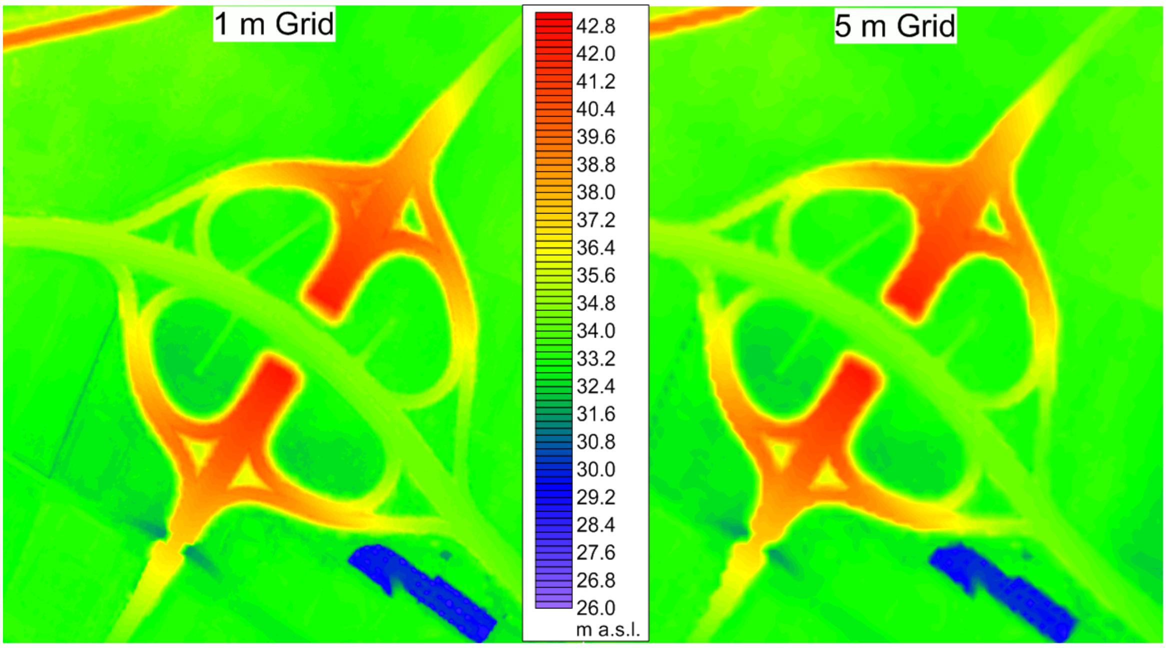

Figure 3. Bathymetry detail of highway intersection with original 1m resolution (left) and with corrected 5m resolution (right).

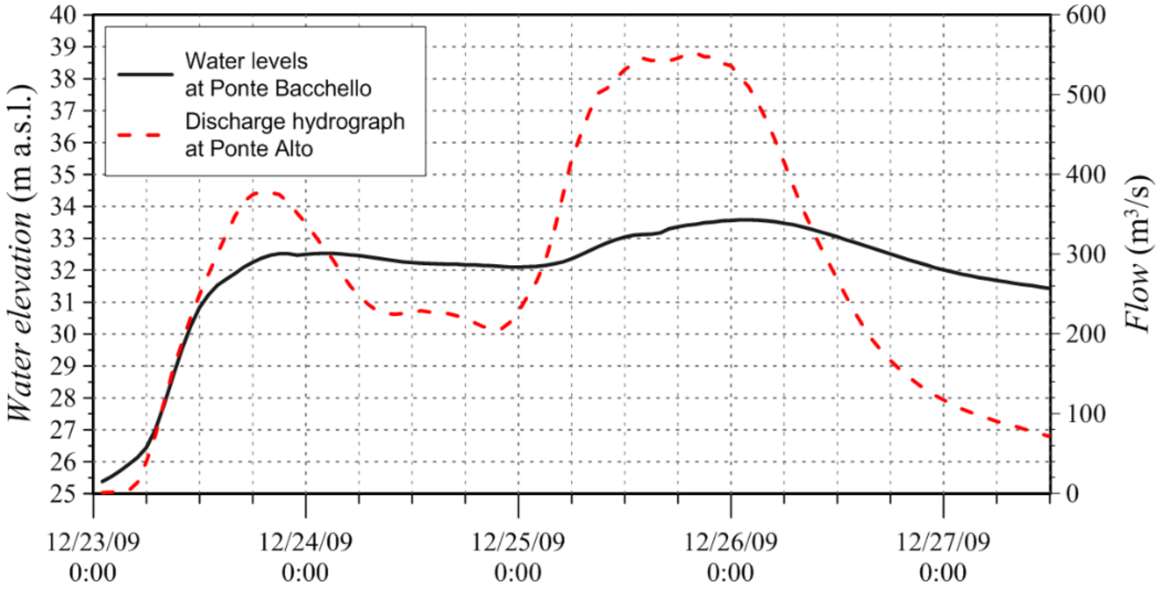

Figure 4. Flow and stage hydrographs of the December 2009 flood event at the gauging stations of Ponte Alto and Ponte Bacchello.

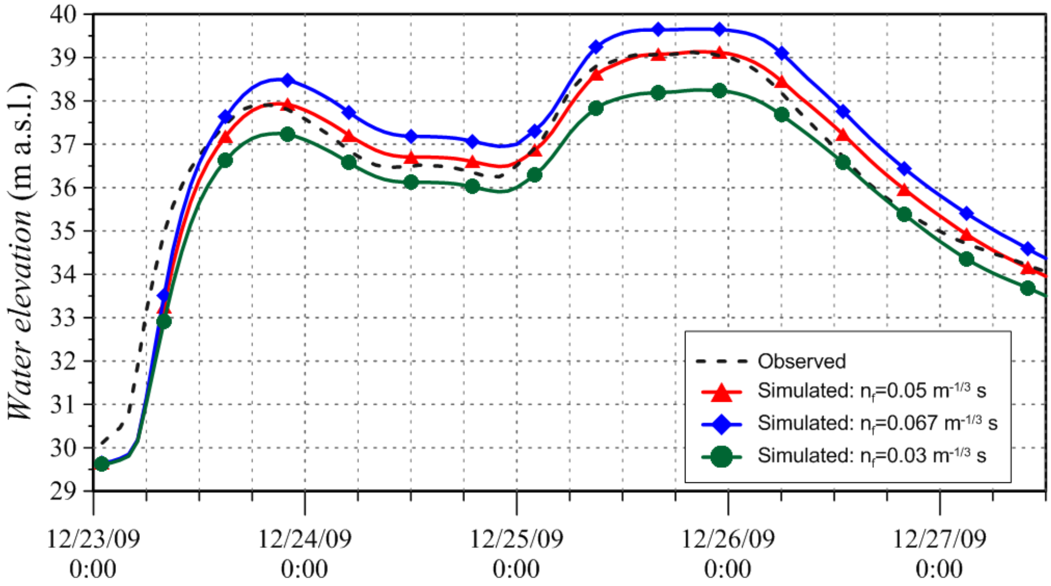

Figure 5. Stage hydrographs at Ponte Alto gauging station for the event of December 2009: comparison between observed and simulated data with different values of roughness.

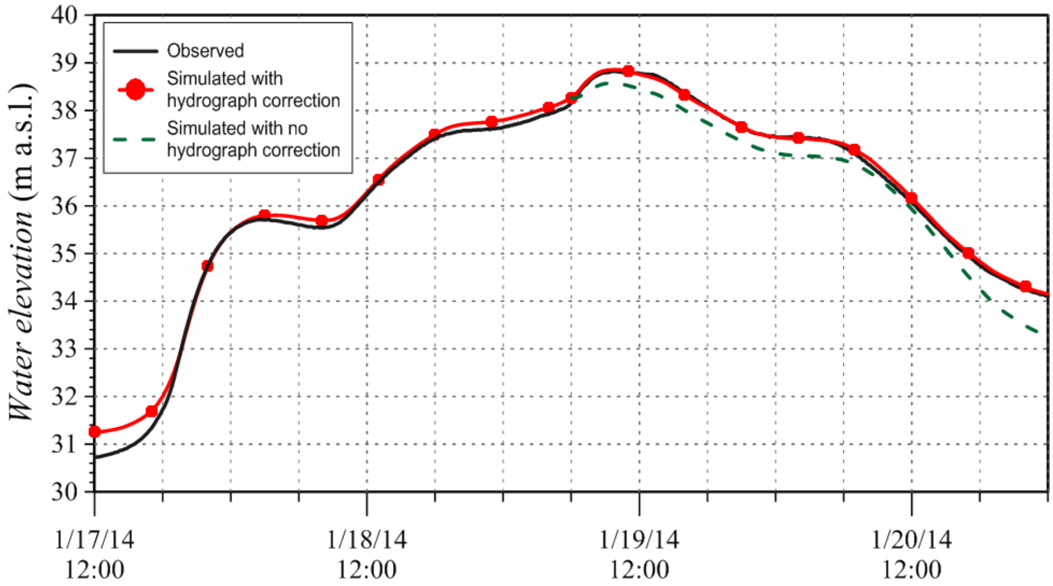

Figure 6. Observed and simulated stage hydrographs at Ponte Alto gauging station for the event of January 2014.

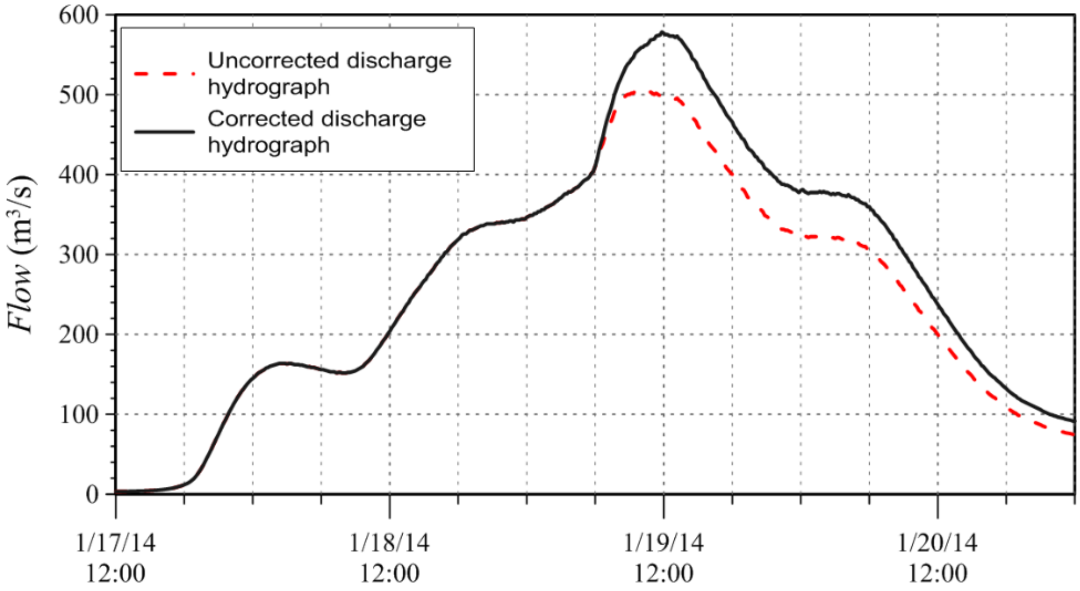

Figure 7. Uncorrected and corrected discharge hydrographs imposed as upstream boundary condition (Ponte Alto) for the flood event of January 2014.

$0.03\ m^{-1/3} \cdot s$	$0.05\ m^{-1/3} \cdot s$	$0.07\ m^{-1/3} \cdot s$
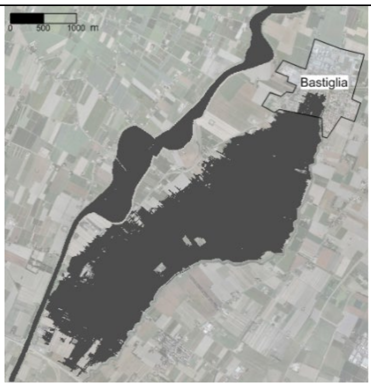		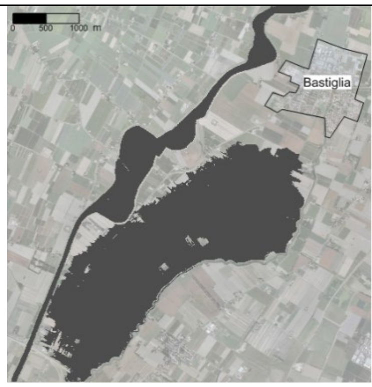

Figure 8. Map of the flooding extent at 0:45 PM on 19th January 2014 for the three simulation in presence of different roughness for the rural areas.

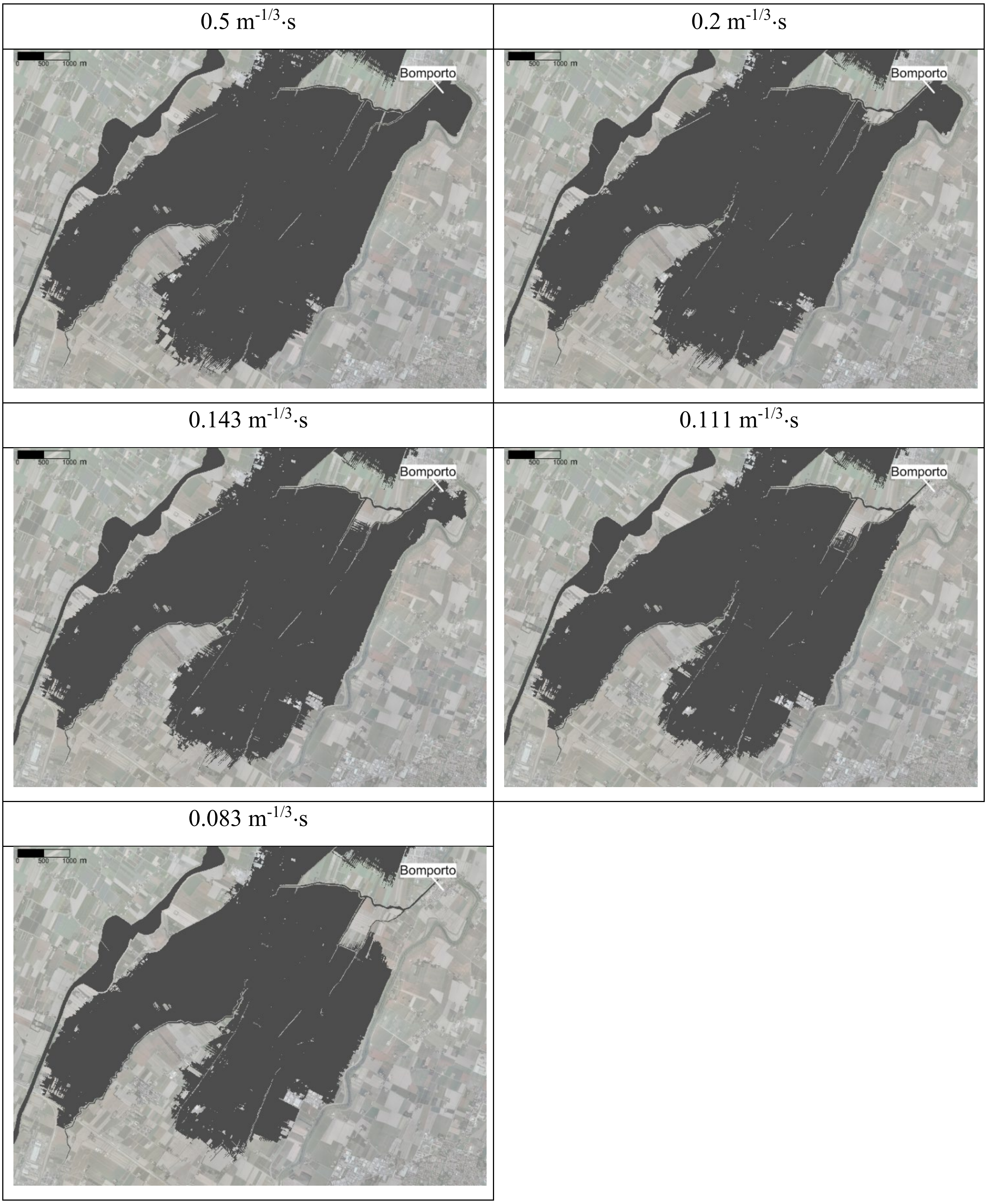

Figure 9. Map of the water depths at 10:30 AM on 20th January 2014 for the five simulations in presence of different roughness for the built-up area areas.

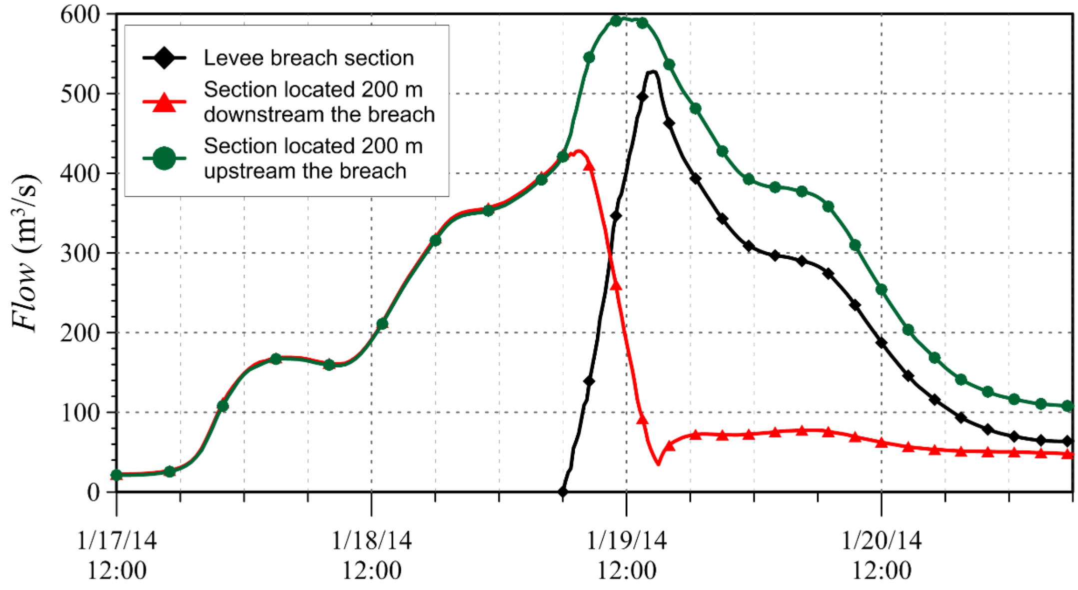

Figure 10. Discharge hydrographs at the sections of the breach, 200 m upstream and 200 m downstream along the river.

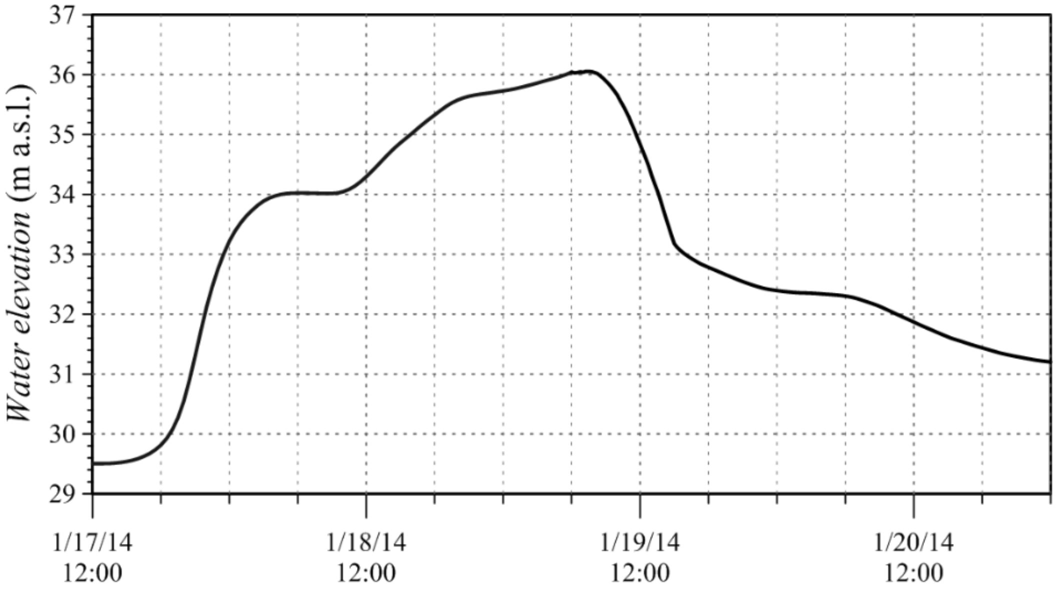

Figure 11. Stage hydrograph referred to a point in the river close to the breach section.

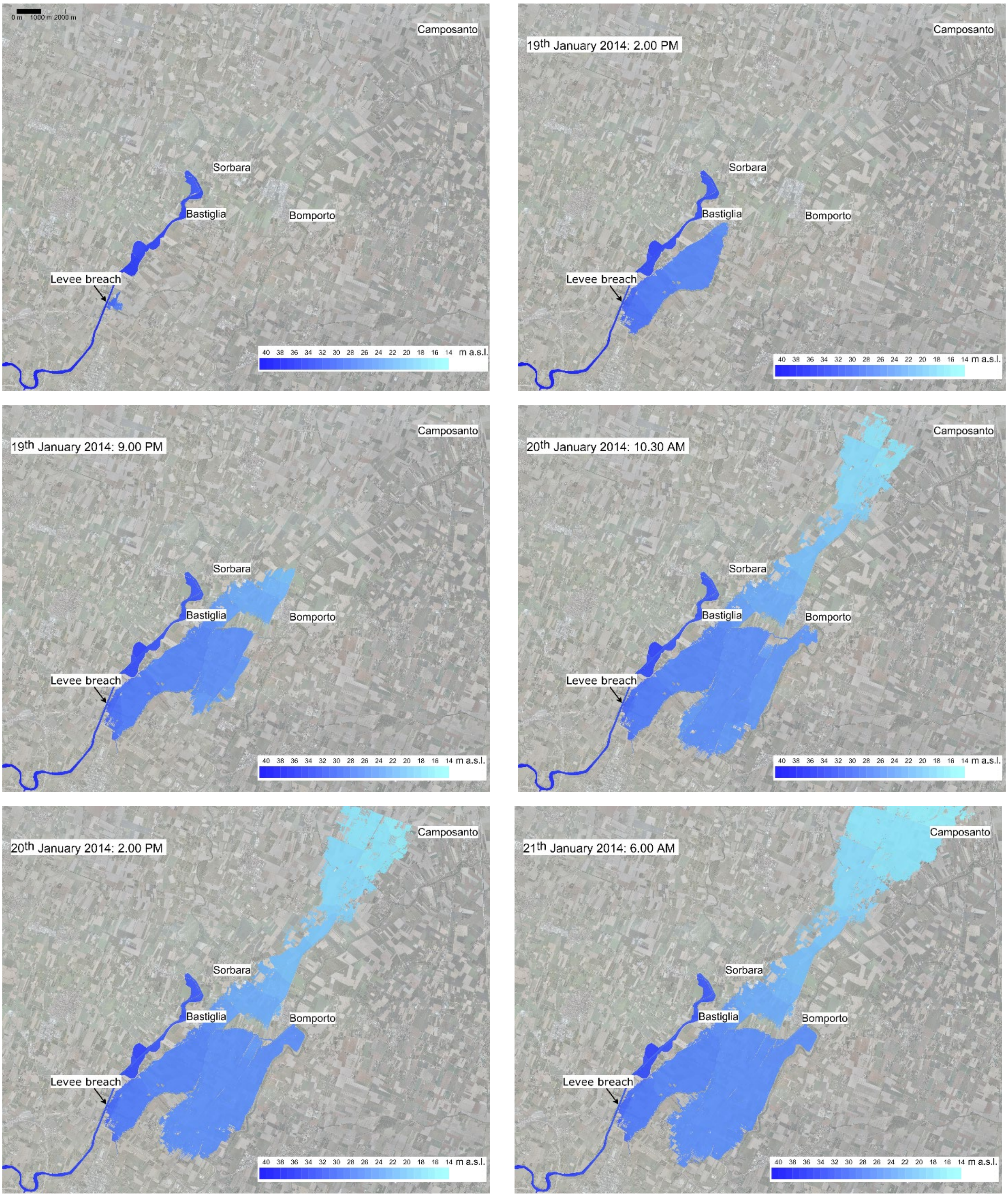

Figure 12. Numerical reconstruction of the flooding event. (a) 1 hour after the bank failure, (b) flooding of Bastiglia, (c) 15 hours after the bank failure, (d) flood wave arrival at Bomporto, (e) 32 hours after the bank failure, (f) 48 hours after the bank failure.

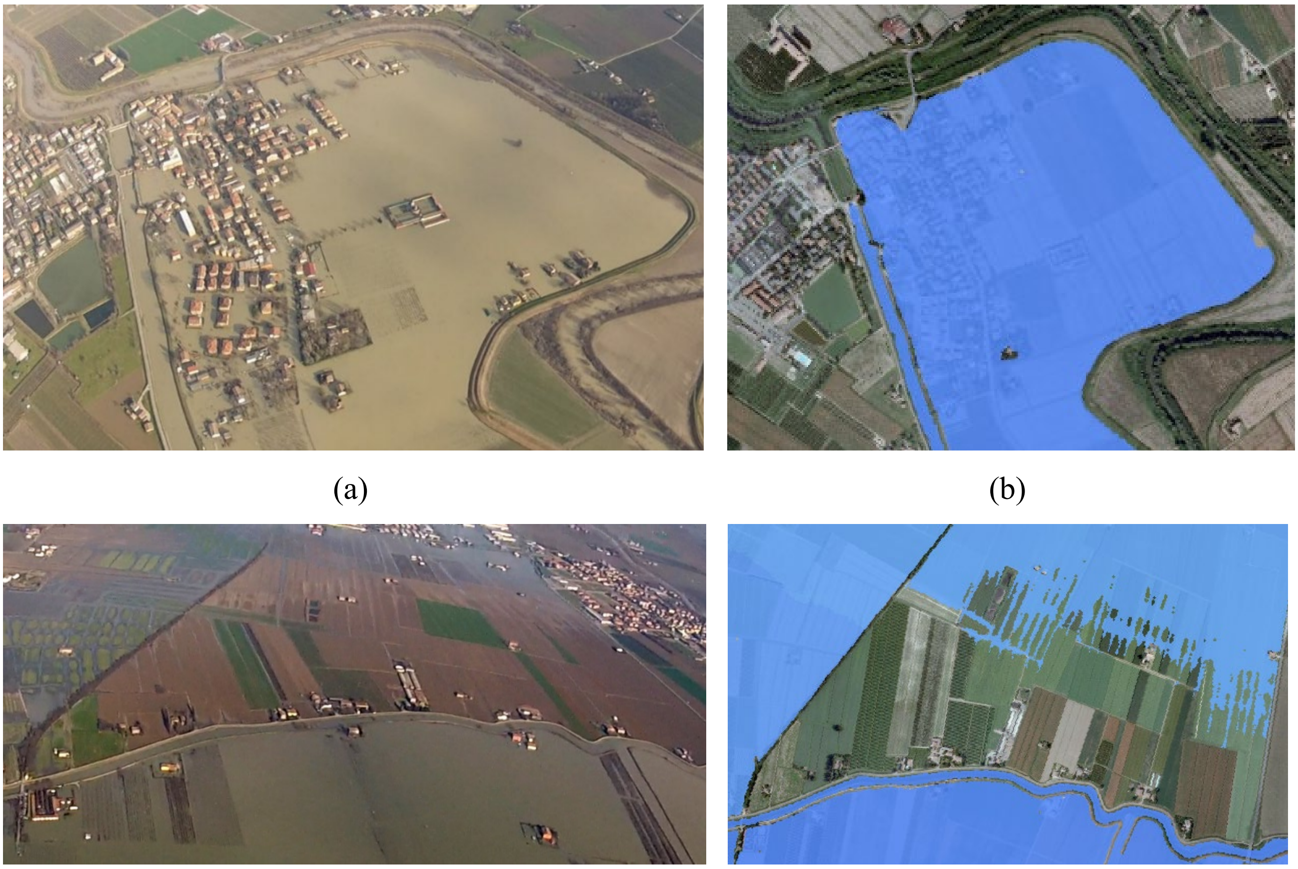

(a) (b)

(c) (d)

Figure 13. Bomporto town, 22nd January 2014 at 1.30 PM: comparison among simulated flooded area (b, d) and aerial views (a, c).

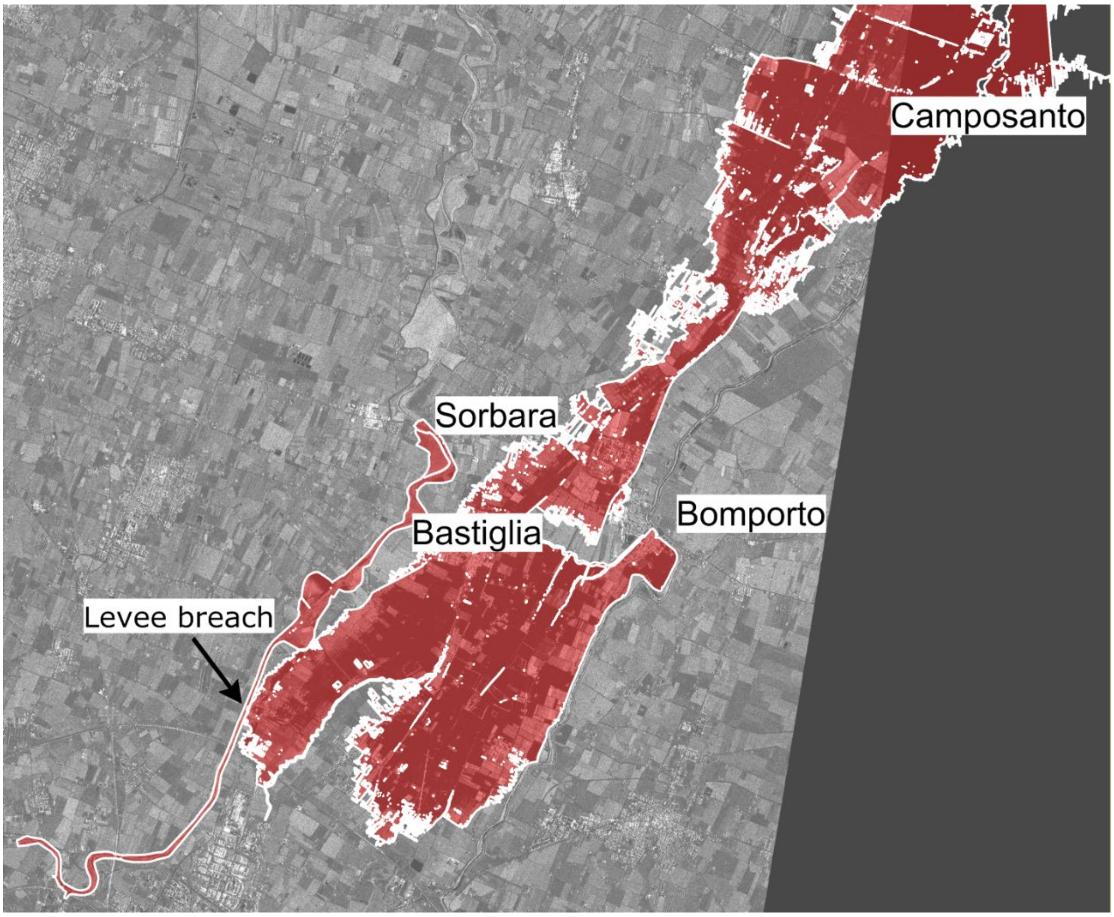

Figure 14. Comparison between the SAR image (foreground) and the simulated flooding (red area).

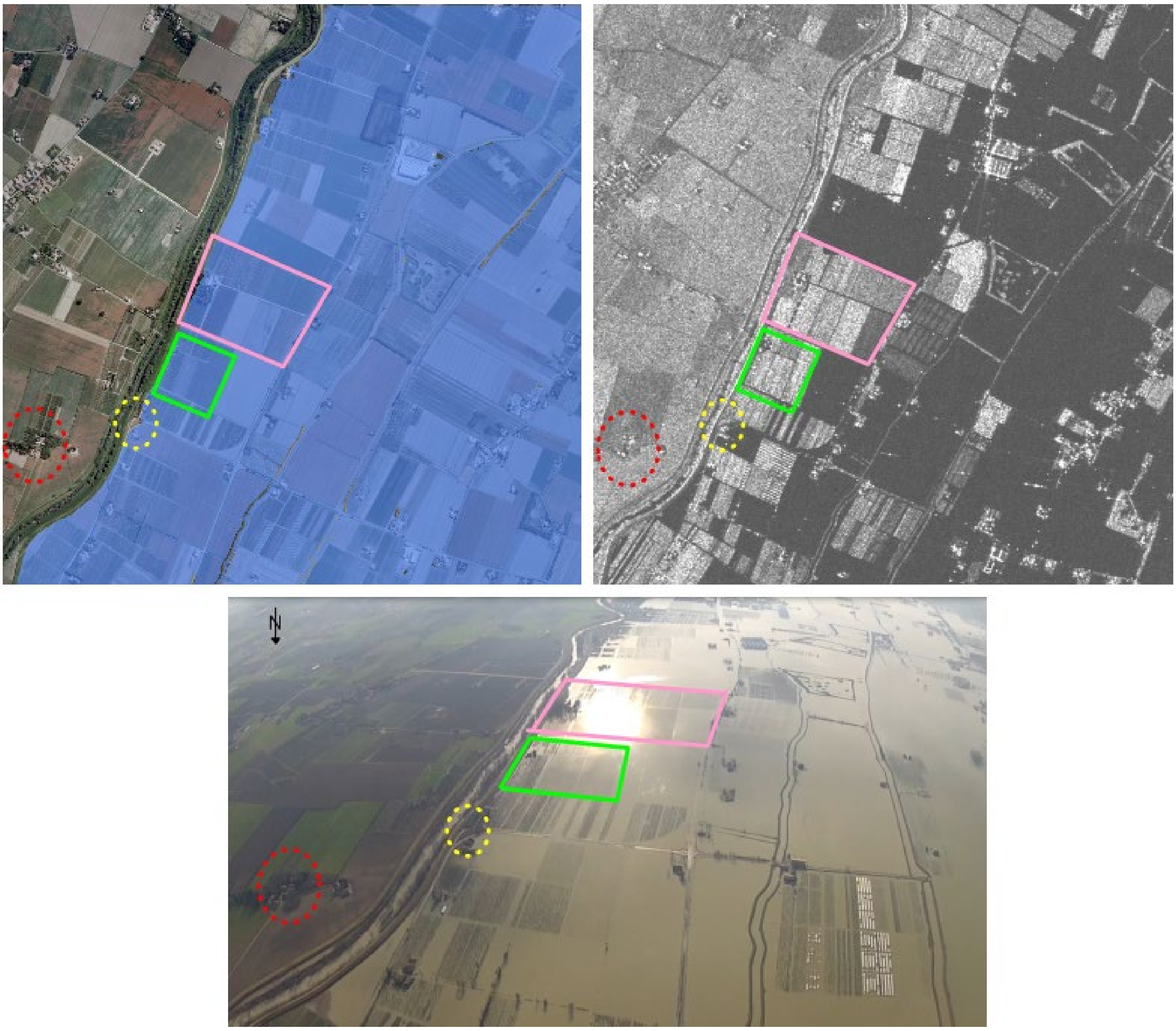

Figure 15. Comparison among computed results, SAR image and aerial image focusing on some parcels of land detected as not flooded in the binary SAR observation for the event under investigation.

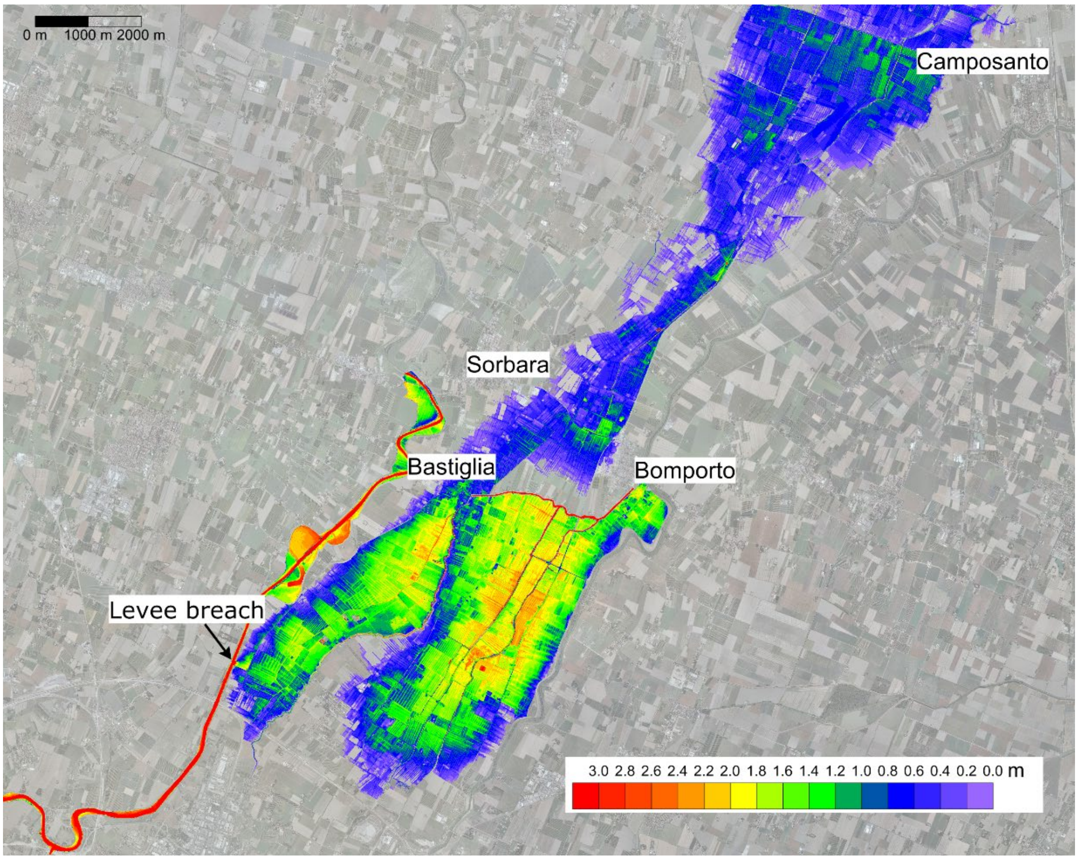

Figure 16. Map of simulated maximum water depths for the January 2014 event

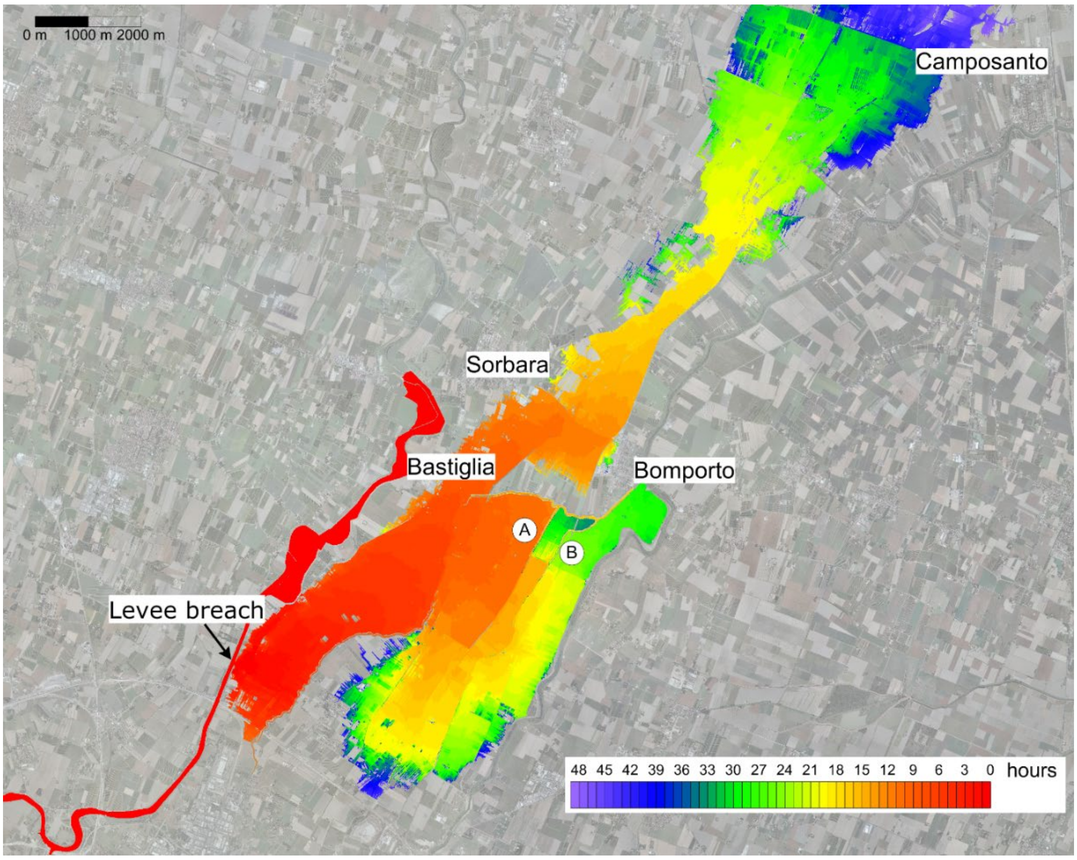

Figure 17. Map of flooding arrival times. Time zero is referred to the opening of the breach.

n_f ($m^{-1/3}\cdot s$)	0.067	0.05	0.03
E_h (-)	86.4	94.2	87.1

Table 1. Nash-Sutcliffe efficiency for the three different roughness coefficients considered